A Discharge Model for Phase Transformation Electrodes: Formulation, Experimental Validation, and Analysis

Chunsheng Wang,*,†,‡ Uday S. Kasavajjula,† and Pedro E. Arce†

Department of Chemical Engineering and Center for Manufacturing Research, Tennessee Technological University, Cookeville, Tennessee 38501

Received: June 10, 2007; In Final Form: July 27, 2007

The discharge kinetics of phase transformation electrodes for Li-ion batteries were investigated by developing a mathematical model based on mixed-mode phase transformation, by assuming that the phase transformation is controlled by both Li chemical diffusion and interface mobility. The discharge model was validated by matching the model discharge curves with the experimental discharge curves of two $LiFePO_4$ samples at different current densities. With the validated model as a tool, effects of phase transformation, chemical diffusion, and solid solution range on rate capability were determined and analyzed. The high rate performance of $LiFePO_4$ was well explained by using this model. The model developed here is applicable for any ion insertion electrode with a phase transformation, such as $Li_4Ti_5O_{12}$ in Li-ion battery and metal-hydride electrodes in Ni/MH batteries.

Introduction

Low pulse power and abuse tolerance, high cost, and short cycle life are the critical barriers for the usage of the current Li-ion batteries in hybrid electric vehicles (HEVs) and battery electric vehicles (EVs). One of the key technologies for overcoming these barriers is to develop low-cost and more-stable cathode materials with high rate capability. The $LiFePO_4$ material invented by Goodenough et al.[1] is a very promising choice for cathode materials for HEV and EV Li-ion batteries because of its high theoretical capacity (170 mAh/g), high electrochemical and thermal stability, and its being relatively inexpensive and less toxic in nature compared to $LiCoO_2$. In spite of these advantages, this material is found to have poor rate capability due to its low electronic conductivity (10^{-9}−10^{-10} S/cm),[2−4] poor Li-ion diffusivity,[5] and sluggish phase transformation between the Li-deficient phase (Li_xFePO_4, $x \sim 0.05$) and Li-rich phase (Li_yFePO_4, $y = 0.78-0.95$).[6] Several methods (although the detailed mechanisms are still under debate) have been reported to effectively enhance the rate performance of $LiFePO_4$ cathodes. These include, for example, adding/coating electronic conductive media (carbon,[9] Fe_2P[10]) into/on $LiFePO_4$ and doping other metals[4] in order to enhance the electronic conductivity; synthesizing nanoscale particles[11,12] to shorten the Li transport length; and doping $LiFePO_4$ with Nb[6−8] for increasing the solid solution range of $LiFePO_4$ and thereby improving the phase transformation rate. Though, from the time of invention of $LiFePO_4$, a large improvement in rate capability was achieved, there seems to be some disagreement regarding the controlling factors for its rate capability. Our previous work[5] showed that when the rate of phase transition is fast, $LiFePO_4$ with a high and balanced electronic/ionic conductivity would show a high rate performance. Otherwise, the rate of phase transformation will become a rate-limiting step.[13] Reducing the volume change of phase transformation by increasing the solid solution range was found to improve the rate performance of $LiFePO_4$.[6] The importance of the rate of phase transformation and electronic conductivity is evident from the higher rate capability of $Li_4Ti_5O_{12}$ than that of $LiFePO_4$, in spite of the relatively low Li-ion conductivity ($\sim 10^{-5}$ S/cm)[14] of $Li_4Ti_5O_{12}$. The high rate capability was attributed to the high electronic conductivity of $Li_7Ti_5O_{12}$ (10^{-2} S/cm[15]) formed during charge/discharge of $Li_4Ti_5O_{12}$ and the zero volume difference between $Li_4Ti_5O_{12}$ and $Li_7Ti_5O_{12}$.[16] All previous experimental studies confirmed that the rate of phase transformation[6−8,13] plays an important (even a critical) role in the charge/discharge behavior of $LiFePO_4$. However, due to the lack of a theoretical study on the kinetics of $LiFePO_4$, the role of mixed (ionic and electronic; referred to as chemical diffusion in the literature[6]) diffusion and that of phase transformation on charge/discharge behavior as well as methods to further improve the rate performance of $LiFePO_4$ are still not clear and need further investigation.

Combining the theoretical model with experiments is very useful to understand the reaction mechanism of $LiFePO_4$. Recent microstructural characterizations showed that the $LiFePO_4$ particles are of a plate-like shape and that the Li-ion diffusion takes place largely in one dimension.[18] Therefore, the rectangular geometry of the shrinking-core model has been used in this contribution to capture the behavior of the discharge process of the Li-ion battery material. In addition, the rate of phase transformation of $LiFePO_4$ has been found to be slow,[13] and it is assumed in the present work that the discharge/charge process may be controlled by both diffusion and rate of phase transformation. This approach differs from previous contributions,[17,19] where the spherical geometry of shrinking-core model was used and only diffusion was considered to be the rate-limiting step. In the model development section of this contribution, it will be shown that the shrinking-core model[17,19] is a limiting case of the present model.

In the present work, a generalized model including electronic conductivity, Li-ion diffusivity, and phase transformation rate

* To whom correspondence should be addressed. E-mail: cswang@umd.edu. Present address: Department of Chemical & Biomolecular Engineering, University of Maryland, Collegel Park, MD 20742.
† Department of Chemical Engineering.
‡ Center for Manufacturing Research.

10.1021/jp074490u CCC: $37.00 © 2007 American Chemical Society
Published on Web 10/04/2007

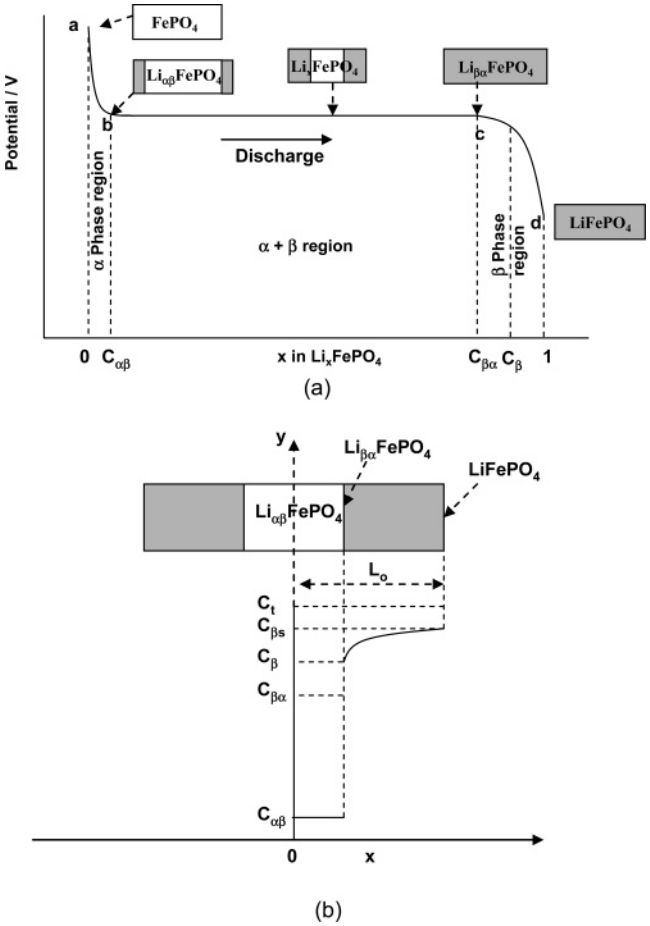

Figure 1. Schematic diagram showing (a) phase transformation and (b) Li concentration distribution during the discharge of a $LiFePO_4$ particle (Li insertion into $FePO_4$).

is developed and validated by using the experimental results of two commercially available $LiFePO_4$ electrodes. With this model as a tool, the effects of Li chemical diffusion, phase transformation rate, and the solid solution range on rate capability are investigated. To the best of our knowledge, this model is the most comprehensive and the first effort to account for the role of phase transformation rate and volume change in modeling the charge/discharge process. Finally, the model developed in this contribution can be used for predicting charge/discharge behavior of other phase change electrodes, thus making it a useful tool for practitioners in the field.

Description of Discharge Process in $LiFePO_4$: General Aspects. The most commonly used conventional crystalline $LiFePO_4$ material was considered for modeling, although the submicrocrystalline $LiFePO_4$ is available as electrode material.[20] The discharge process of the crystalline $LiFePO_4$ electrode can be simply described on the basis of 1D diffusion of the Li ion in the $FePO_4/LiFePO_4$ lattice,[18] because the metastable phase $Li_{0.60}FePO_4$ (if formed during heat treatment) will be decomposed to $LiFePO_4$ and $FePO_4$ after long time aging at room temperature.[21] The lithium concentration distribution of $LiFePO_4$ during discharge is shown in Figure 1. The fully charged $LiFePO_4$ particle consists of a single $FePO_4$ phase, and upon discharge, the following reaction takes place; the detailed process for the discharge is given below:

$$FePO_4 + Li^+ + e^- \rightarrow LiFePO_4 \qquad (1)$$

At the beginning of the discharge, Li inserts into surfaces of the $FePO_4$ particles along the *x*-direction and diffuses into the interior of the particle (Figure 1a). This process results in the formation of a solid solution of Li_yFePO_4 (α phase, Figure 1a), and this process continues until the Li content "*y*" in Li_yFePO_4 reaches the solid solubility limit ($C_{\alpha\beta}$). This process corresponds to the initial potential sloping line in the discharge curve (a−b section in Figure 1a). Further insertion of Li into the lattice leads to the formation of $Li_{\beta\alpha}FePO_4$ (β phase), i.e., the formation of an interface along the two sides of the particle, and the interfaces between β and α phases move toward the center during further Li insertion (b−c section in Figure 1a). This procedure continues until both interfaces reach the center of particle, i.e., when the particle is fully formed of $Li_{\beta\alpha}FePO_4$ (β phase, c point in Figure 1a). Further discharge leads to further diffusion of Li ion into the particle and conversion of $Li_{\beta\alpha}FePO_4$ (β phase) to $LiFePO_4$ (c−d section in Figure 1a).

Figure 1b shows the Li concentration in a planar geometry for $LiFePO_4$ during the discharge process. As in the previous shrinking-core model,[17] the lithium content of the α phase at the interface is also assumed to be equal to the equilibrium concentration $C_{\alpha\beta}$. The reason behind this assumption is because the Li concentration in the α phase reaches equilibrium during the resting time before discharge and also the lithium solubility (or discharge capacity) in the α phase is very small. However, the concentration of the β phase (C_β) at the interface is higher than the equilibrium concentration of the β phase ($C_{\beta\alpha}$) due to the low interface mobility,[22] which is different from the original shrinking-core model.[17,19] This concentration departure is required to drive the interface movement because of the nonequilibrium conditions prevailing at the interface. The lithium required for the $\alpha \rightarrow \beta$ phase transformation is provided by the chemical diffusion of lithium from the surface to the interface due to the concentration gradient present in the β phase. The surface concentration of β phase ($C_{\beta s}$) during discharge is always higher than the interface concentration (C_β) (Figure 1b) and becomes equal to the maximum lithium concentration in the $FePO_4$ lattice (C_t) at the end of discharge. If the rate of the interfacial reaction is fast and the phase transformation is governed by the chemical diffusion of lithium in the β phase, the interface concentration (C_β) will be near to the equilibrium value $C_{\beta\alpha}$. This is known as the diffusion-controlled growth, and it was modeled by Srinivasan et al.[17] and Zhang et al.[19] using the shrinking-core model in spherical geometry. However, if the rate of the interfacial reaction is slow, the growth rate will be governed by the interface kinetics; i.e., the phase growth is interface-controlled.[23] In the most of the phase transformations, both the interface reaction and the diffusion process affect the phase growth. Therefore, such a transformation can be described by the mixed-control or the mixed-mode phase transformation.[24] Also, the concept of mixed-mode phase transformation has been successfully applied in the modeling of dissolution of spherical precipitates[25] and in proeutectoid growth in Fe−C alloys.[24,26,27]

Model Development Based on the Mixed-Mode Phase Transformation. The lithium diffusion process in $LiFePO_4$ during the discharge process can be modeled by modifying the transport equations proposed by Srinivasan et al.[17] based on the mixed-mode phase transformations. In the present model, the interfacial concentration C_β is used to replace the equilibrium concentration $C_{\beta\alpha}$ and the transport equations are considered in rectangular coordinates instead of spherical coordinates. The interface concentration C_β is calculated by performing a flux balance of Li^+ ions toward the interface and across the

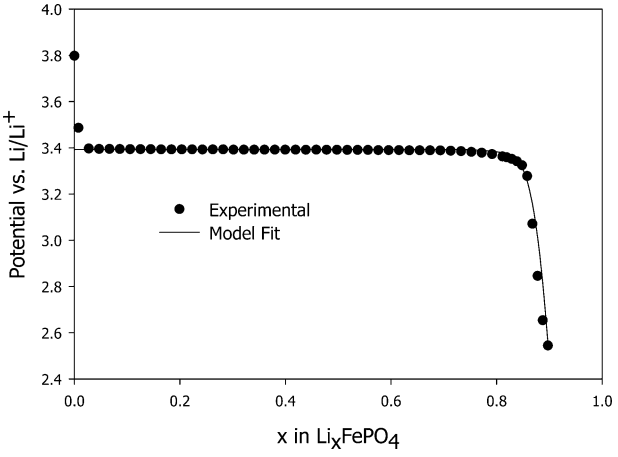

Figure 2. Equilibrium potential vs Li content x in Li_xFePO_4/A obtained from experiment and eq 8.

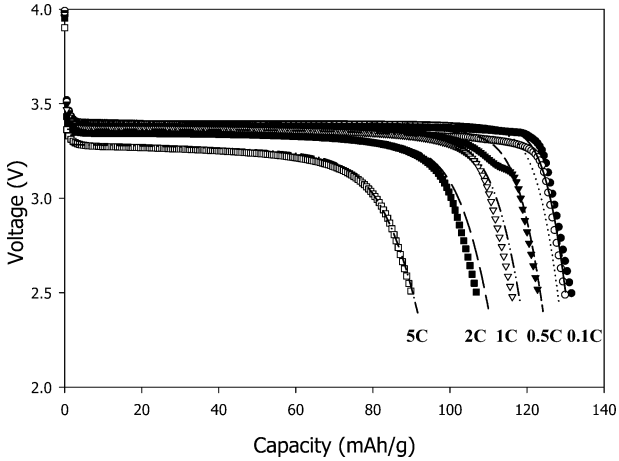

Figure 3. Discharge curves of $LiFePO_4$/A obtained from experiments and model at 5, 2, 1, 0.5, 0.2, and 0.1 C: symbols, experiments; lines, model.

interface.[22] The theory of mixed-mode phase transformations and the calculation of C_β are discussed in the supporting information due to the space limitation. The governing equations, initial condition, and boundary conditions for this model can be written as follows:

$$\frac{\partial C}{\partial t} = D\left(\frac{\partial^2 C}{\partial x^2}\right) \tag{2}$$

$$C = C_{\alpha\beta} \qquad \text{at} \qquad t = 0 \tag{3}$$

$$D\left(\frac{\partial C}{\partial x}\right) = \frac{i}{F} \qquad \text{at} \qquad x = x_0 \tag{4}$$

$$C = C_\beta = \frac{1}{2}\left[C_{\beta\alpha} + C_{\alpha\beta} + \sqrt{(C_{\beta\alpha} - C_{\alpha\beta})^2 - \frac{4C_{\beta\alpha}D}{MRT(1 - A \times (1 - x_i(t)^{2.2}))}\left(\frac{\partial C}{\partial x}\right)_{x = x_i}}\right] \qquad \text{at} \qquad x = x_i(t) \tag{5}$$

$$\frac{dx_i(t)}{dt} = \frac{D}{(C_{\alpha\beta} - C_\beta)}\left(\frac{\partial C}{\partial x}\right)_{x = x_i(t)} \tag{6}$$

When the interface reaches the center of the particle (the dimensionless interface position reaches a value of 0.001), eqs 5 and 6 are replaced by the following equation

$$D\left(\frac{\partial C}{\partial x}\right) = 0 \qquad \text{at} \qquad x = 0 \tag{7}$$

where C, in the system of equations, corresponds to the concentration of lithium inside the Li_xFePO_4 particle; $C_{\alpha\beta}$ corresponds to the concentration of the Li-deficient phase; C_β corresponds to the actual interface concentration of the Li-rich phase; D corresponds to the lithium chemical diffusion coefficient (electron and ionic) in the Li-rich phase, which is assumed to be concentration independent; $x_i(t)$ corresponds to interface position, and i corresponds to the reaction current applied on the particle surface; M corresponds to the interface mobility, which depends on the degree of coherence of the interface buildup of stress and deformations; and A corresponds to the accommodation energy factor associated with the volume change. Since the accommodation energy induced by the volume change (occurring during the phase transformation) reduces the rate of phase transformation,[28] A value will increase with the increase in volume change of phase transformation and it is expected to lie between 0 and 1. The parameter n determines the type of variation in accommodation energy during the progress of transformation; an n value close to 1 corresponds to a linear increase in the accommodation energy. When the n value increases further, the accommodation energy increases quickly during the initial stages of transformation and reaches steady state.

Here, it should be noted that when the interface mobility is very fast ($M \rightarrow \infty$), C_β in eqs 5 and 6 will be equal to the equilibrium concentration $C_{\beta\alpha}$. In such a case, the system of equations corresponds to diffusion-controlled phase transformation, which has been modeled by Srinivasan et al.[17] Therefore, the Srinivasan model is a limiting case of the present model under the assumption that the rate of the interfacial reaction is very fast. To simplify the calculation, eqs 2−7 are converted to a dimensionless form by using the procedure mentioned in ref 17. Thus, the system of equations in the dimensionless form corresponds to a nonlinear moving boundary value problem. This differential model was solved by using the numerical method of lines (MOL) approach.[29,30] In the numerical MOL, the system of equations is described in the space domain, thereby converting the system of partial differential equations into a system of differential-algebraic equations (DAE). The resulting system of differential-algebraic equations is then solved by using time-integration techniques. Details on the MOL can be found elsewhere[29,30] and will not be repeated here.

Experimental Section

Two different carbon coated $LiFePO_4$ materials ($LiFePO_4$/A and $LiFePO_4$/B) as received from industries were used in this study. The $LiFePO_4$ active material was mixed with different amounts of carbon black (0, 5, and 10 wt %) and 10 wt % poly(vinylidene fluoride) (PVDF, Kynar, Elf-Atochem) in 1-methyl-2-pyrrolidinone solvent to form a viscous paste, which was then homogenized in an ultrasonic bath for 30 min. The paste obtained by this procedure was coated on a carbon coated Al foil using a doctor blade. The film was then dried in a vacuum oven at 120 °C for 12 h. After the material was cooled to room temperature, the sheet was rolled and then cut into square pieces of 3 cm length, which were used as electrodes. The active material loading on the electrode was about 5 mg/cm^2. Two $LiFePO_4$/A electrodes with and without 10 wt % carbon addition were used for measuring exchange current density using

TABLE 1: List of Parameter Values Used for Modeling $LiFePO_4$ Cathode Materials and for Further Analysis

parameter	$LiFePO_4$ sample A	$LiFePO_4$ sample B	analysis
length of the $FePO_4$ particle ($2L_0$) (μm)	0.8	0.8	0.8
density of $FePO_4$ particle (ρ) (g/cm^3)	3.6	3.6	3.6
Li chemical diffusion coefficient (D) (m^2/s)	8×10^{-14}	3.2×10^{-13}	5×10^{-17} to 3.2×10^{-13}
interface mobility (M) (mmol/(J s))	1.3×10^{-11}	1.85×10^{-10}	3×10^{-12} to 1.3×10^{-8}
dimensionless equilibrium concentration of Li-rich phase ($C_{\beta\alpha}/C_t$)	0.77	0.85	0.1−0.77
exchange current (i_0) (A/g)	0.1	0.25	0.1
accommodation energy factor (A)	1.0	1.0	0.0−1.0
n	2.2	2.2	2.2
C_t (mol/cm^3)	0.02044	0.02119	0.02044

electrochemical impedance and linear polarization (1mv/s) at 50% state of discharge, while $LiFePO_4$/A and $LiFePO_4$/B electrodes (containing 5 wt % carbon) were used for obtaining equilibrium discharge potential−composition isotherms (PCI) as well as discharge curves at different current densities. The equilibrium discharge PCIs at room temperature were measured in a three-electrode pouch cell using a galvanostatic intermittent titration (GITT) technique at a low current density of 0.02 C. The electrodes were charged and discharged by using a series of intermittent current values for 1.0 h and leaving the electrode at an open circuit for 2.0 h between each intermittent current value to reach a constant potential. The discharge capacity of the cell (sample A) obtained from this test is 150 mAh/g.

The electrochemical performance of two $LiFePO_4$/5 wt % carbon electrodes was determined using a coin cell (CR 20). All the cells were assembled in an argon-filled glovebox, which consisted of $LiFePO_4$/5 wt % carbon as the cathode (working electrode), lithium foil as the anode (and the reference electrode for a pouch cell), 1.0 M $LiPF_6$ in ethylene carbonate/diethyl carbonate/dimethyl carbonate/ethyl methyl carbonate (EC/DEC/DMC/EMC, 1:1:1:3 by volume) (Ferro Corporation) as the liquid electrolyte, and polypropylene (PP) microporous film as the separator. Before testing the electrochemical performance, all the cells were activated through several charge/discharge cycles with a small current (0.1 C, 1 C = 150 mA/g for all the materials studied) using an Arbin Corporation (College Station, TX) automatic battery cycler.

Parameter Estimation of Sample A. *Equilibrium Potential.* Figure 2 shows the equilibrium potential versus Li content curves obtained from GITT experiments for $LiFePO_4$/A. The Li content x in Li_xFePO_4 is calculated by dividing the capacity with the theoretical capacity ($x = 1$ for $C_t = 170$ mAh/g) of the electrode. The equilibrium potential curve consists of two descending curves connected by a long plateau. The long plateau corresponds to the phase change region, and the two descending curves correspond to the solid solution. To use these data in the model, an empirical relation between equilibrium potential and state of discharge was obtained by a curve fitting. The equation is

$$U = 3.3929 - 0.5 \times \exp\left(-\frac{1.55}{\left(\frac{C_{\beta S}}{C_t}\right)^5} + \left(\frac{C_{\beta S}}{C_t}\right)\right) - 8 \times \exp\left(-\frac{0.52}{\left(\frac{C_{\beta S}}{C_t}\right)^{14}}\right) \quad (8)$$

From Figure 2, a close match between experimental results and the model can be found. As indicated in the modeling assumption ($C_{\alpha\beta} = 0$, Figure 1), the initial solid solution curve is not accounted for by eq 8. Due to this fact, the concentration of the lithium-deficient phase in the model can be taken as zero; this assumption simplifies the equations. The lithium concentration at the surface, obtained by solving the system of equations, is fed into eq 8 and the equilibrium potential as a function of time is calculated. C_t in eq 8 corresponds to the maximum concentration of lithium that can be incorporated into the $FePO_4$ lattice (0.02044 mol/cm^3); this value is calculated from Faraday's law. Also, from the Figure 2, the equilibrium concentration of the Li rich phase is found to be 0.771×0.02044 mol/cm^3.

Overpotential and Exchange Current. Overpotential can be calculated using the following equation[31]

$$i = i_0\left(\frac{(C_t - C_{\beta s})}{(C_t - C_{\beta\alpha})} \times \exp\left(\frac{\alpha F\eta(t)}{RT}\right) - \frac{C_{\beta s}}{C_{\beta\alpha}} \times \exp\left(-\frac{F\eta(t)}{RT}\right)\right) \quad (9)$$

where i_0 is the exchange current. The voltage of the $LiFePO_4$ electrode is calculated by adding the overpotential to the equilibrium potential. The exchange current densities of pure $LiFePO_4$/A and $LiFePO_4$/A with 10% of carbon black electrodes were measured at the 50% state of discharge using linear polarization and electrochemical impedance spectroscopy (EIS) experiments. From both the experiments, the i_0 value was found to be 0.3 A/g for $LiFePO_4$/A containing 10% carbon black and 0.007 A/g for pure $LiFePO_4$/A. Since the $LiFePO_4$ used for this study has 5% carbon black (which lies between the above mentioned two samples), an exchange current density of 0.1 A/g is used for simulation.

Parameter Estimation for $2L_0$, ρ, α, A, D, M, and n. For all the simulations, the particle radius ($2L_0$) was taken as 0.8 μm according to SEM observation; the value is similar to the one reported in the literature.[32] The density (ρ) value (3.6 g/cm^3) and transfer coefficient (α) value (0.5) were taken from the literature.[17] Since the effect of the accommodation energy on the phase transformation is not known, the value of A was taken as 1 considering this as the base case, and it will decrease with the decrease in volume change (see later sections). Since the experimental determination of accurate values of diffusion coefficient and interface mobility is difficult, the values of these parameters are extracted by fitting the model to the experimental discharge curves at 2 and 5 C in Figure . The end of discharge values at 5 and 2 C were used to estimate the parameter n. By using this procedure, the fitted values for D, M, and n were found to be 8×10^{-14} m^2/s, 1.3×10^{-11} mmol/(J s), and 2.2, respectively.

Parameter Estimation of Sample B. Similarly, the experimental discharge curves at 20 and 10 C for sample B were used to estimate the values of D, M, and n of sample B. The values of the parameters used in this simulation for samples A and B are listed in Table 1. The methodology adopted here for parameter estimation and model validation is similar to earlier works published in the literature.[17,19,33]

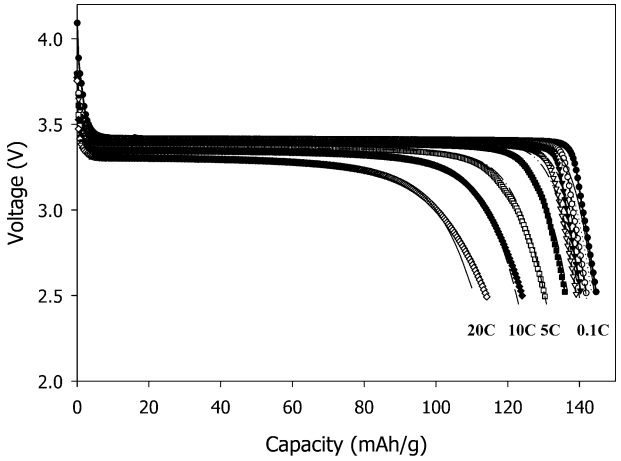

Figure 4. Discharge curves of $LiFePO_4$/B obtained from experiments and model at 20, 10, 5, 2, 1, 0.5, 0.2, and 0.1 C: symbols, experiments; lines, model.

Model Validation. The model was validated by (1) comparing the calculated discharge curves at different current densities (1, 0.5, 0.2, and 0.1 C) using parameters estimated from fitting experimental discharge curves at other currents (2 and 5 C) with experimental discharge curves at the same current (1, 0.5, 0.2, and 0.1 C), (2) simulating and comparing with experimental discharge, of two $LiFePO_4$ samples which have a large difference in rate performance, and (3) comparing the current model at high interface mobility ($M \rightarrow \infty$) with a conventional shrinking-core model. Figure 3 shows the discharge curves for $LiFePO_4$/A at different currents (0.1−5 C) obtained from the experiments and model predictions. Plateau potentials, end of discharge values, and discharge curves obtained from the model seem to match well with the experimental results at all currents. By use of the estimated parameter values, for sample B in the model, the discharge curves at 5, 2, 1, 0.5, 0.2, and 0.1 C were obtained and were also compared with the experimental discharge curves as shown in Figure 4. From the comparison of experimental and model discharge curves for samples A and B, one can see a strong validation of the model in predicting the discharge behavior. Apart from this, when the interface mobility is changed to 1.3×10^{-7} mmol/(J s), the model predictions for discharge behavior at different currents were similar to the discharge behavior predicted from the shrinking-core model proposed by Srinivasan et al.[17] This strongly supports the applicability of the model to a wide range of electrodes whose discharge process is controlled by either diffusion or rate of phase transformation. From the comparison of the parameter values for samples A and B in Table 1, the high rate capability of sample B than that of sample A can be attributed to the large increase in interface mobility combining with a moderate increase in diffusion capability.

Effect of Lithium Chemical Diffusion and Interface Mobility on Rate Capability. *Range of $LiFePO_4$ Chemical Diffusion Coefficient.* Since the lithium and the electron in $LiFePO_4$ are envisioned to form a dilute binary electrolyte,[33] the chemical diffusion coefficient D (total lithium ion and electron) can be obtained by following equation:[33]

$$D = \frac{2D_{Li}D_e}{D_{Li} + D_e} \tag{10}$$

where D_{Li} and D_e are the diffusion coefficients of Li ion and electron, respectively. Similarly, the total conductivity (σ) of the lithium ion and the electron can be obtained based on the Nernst−Einstein equation.[34]

$$\sigma = \frac{2\sigma_{Li}\sigma_e}{\sigma_{Li} + \sigma_e} \tag{11}$$

The total conductivity of $LiFePO_4$/A calculated from electronic conductivity[14] (5×10^{-4} S/cm) and ionic conductivity[14] (1.5×10^{-5} S/cm) is found to be 2.9×10^{-5} S/cm. On the basis of the relationship between conductivity and diffusion coefficient of $LiFePO_4$ proposed by Whittingham et al.,[34] the total diffusion coefficient of $LiFePO_4$ is found to be 10^{-13} m^2/s; this value is within the range $10^{-11}-10^{-13}$ m^2/s determined from Mossbauer spectroscopy,[37] although it is slightly lower than the calculated (theoretical) value[34] of 10^{-11} m^2/s and much higher than the value of 10^{-18} m^2/s determined from GITT,[35] cyclic voltammetry[36] (CV), and EIS.[35] The low value for the diffusion coefficient measured from EIS, GITT, and CV is due to the slow phase transformation, because the diffusion coefficient measured here is actually an "effective" diffusion coefficient, which is influenced by phase transformation. EIS, GITT, and CV for the measurement of the diffusion coefficient were proven to be valid only for solid solution reactions.[35] To investigate the effects of chemical diffusion coefficient on the discharge kinetics of $LiFePO_4$, the range for the Li chemical diffusion coefficient for our simulations was chosen to be 3.2×10^{-13} to 5×10^{-17} m^2/s, and these values covered almost the entire range of data reported for diffusion coefficient values.

Range of Interface Mobility M. The range of M values used in this simulation for $LiFePO_4$ was determined by comparing it with the phase transformation in Ti alloy and steel at 720 °C; this has been well studied using the mixed-control model.[27] Sietsma et al. reported M values of 10^{-12} mmol/(J s) for Ti alloys and 10^{-9} mmol/(J s) for steel.[27] Since the phase transformation rate of $LiFePO_4$ under potential-step chronoamperometry (PSCA) at room temperature[13] lies between the phase transformation of Ti alloy and steel at 720 °C,[27] the interface mobility range of 3×10^{-12} to 1.3×10^{-8} mmol/(J s) was considered for the simulation.

Controlling Factors for Rate Capability. To determine the controlling factors for rate capability, the discharge capacities of $LiFePO_4$ at 0.1 and 5 C were obtained by using this model with the chemical diffusion coefficient and the interface mobility varying in the selected range ($D = 5 \times 10^{-17}$ to 3.2×10^{-13} m^2/s; $M = 3 \times 10^{-12}$ to 1.3×10^{-8} mmol/(J s)) while keeping all the other parameters the same as those of sample A. From the discharge capacities at 0.1 and 5 C for each D and M value, the discharge rate capability at 5 C (ratio of the discharge capacity at 5 C to the discharge capacity at 0.1 C) was calculated. Figure 5 shows 3D graphs for the discharge capacity at 0.1 and 5 C as a function of interface mobility and chemical diffusion coefficient. Figure 6 shows contour plots for rate capability at 5 C as a function of interface mobility and chemical diffusion. The results for a micron-sized $LiFePO_4$ particle with $C_{\beta\alpha} = 0.77$ in Figures 5 and 6 can be summarized as follows. (1) To achieve a high discharge capacity and a high rate capability, the chemical diffusion coefficient of $LiFePO_4$ should be higher than 2×10^{-15} m^2/s and the interface mobility should be higher than 1.3×10^{-11} mmol/(J s), because the discharge capacity at 0.1 C (Figure 5a) and the rate capability of $LiFePO_4$ (Figure 5b) begin to drop rapidly when the two parameters fall below these critical values. When the chemical diffusion coefficient is lower than 2×10^{-15} m^2/s, the interface mobility does not have any influence on the rate capability (Figure 6);

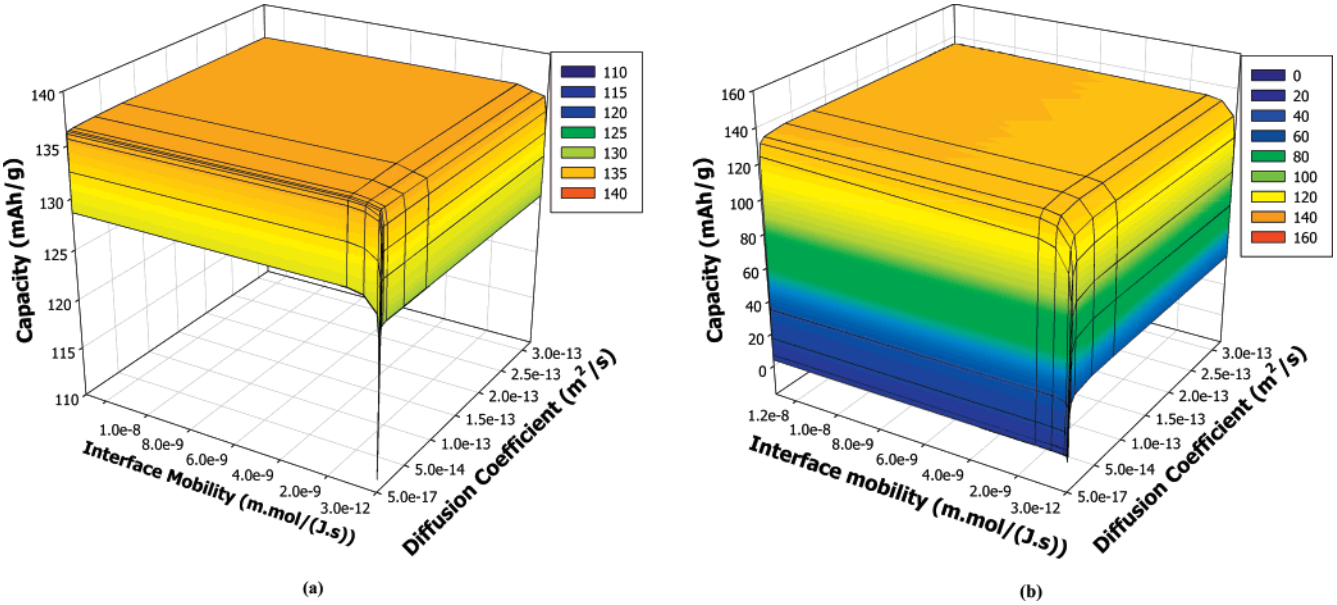

Figure 5. Simulated discharge capacity of $LiFePO_4$/A at different currents as a function of interface mobility and Li chemical diffusion coefficient: (a) 0.1 C; (b) 5 C.

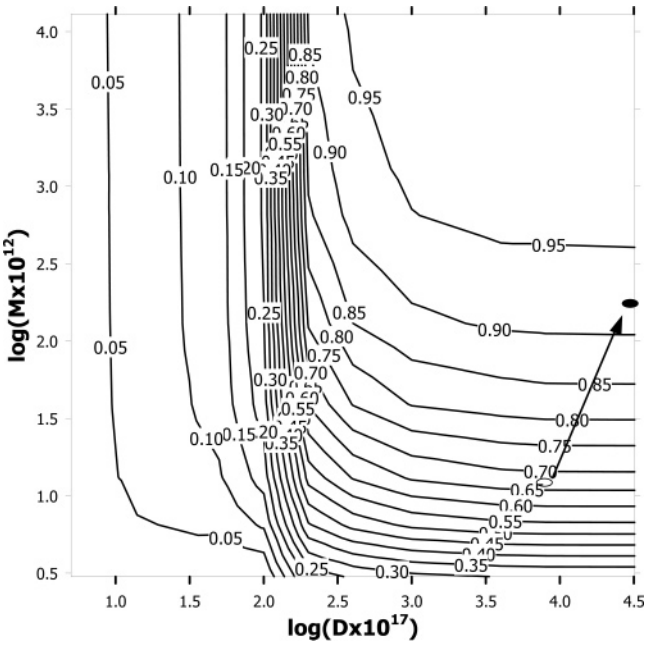

Figure 6. Contour plot for the ratio of discharge capacity (simulated) at 5 C to the discharge capacity (simulated) at 0.1 C for $LiFePO_4$ as a function of interface mobility and chemical diffusion. The capacity ratio for sample A (filled circle) and sample B (empty circle) are also shown for comparison.

i.e., the discharge process is controlled by diffusion. (2) On the basis of the estimated values of diffusion coefficient and interface mobility, the positions of the samples A and B were marked on the rate capability contour plot (Figure 6). From Figure 6, it is clear that the rate capability at 5 C for sample A can only be improved by increasing the interface mobility, which implies that the discharge process at 5 C is controlled by the interface mobility. Similar conclusions can be drawn for sample B. The higher rate performance of sample B than that of sample A is mainly due to the fast interface mobility with slight contribution from the improved diffusion coefficient. (3) The contour plot shown in Figure 6 is extremely useful, as it shows the required diffusion coefficient and interface mobility values

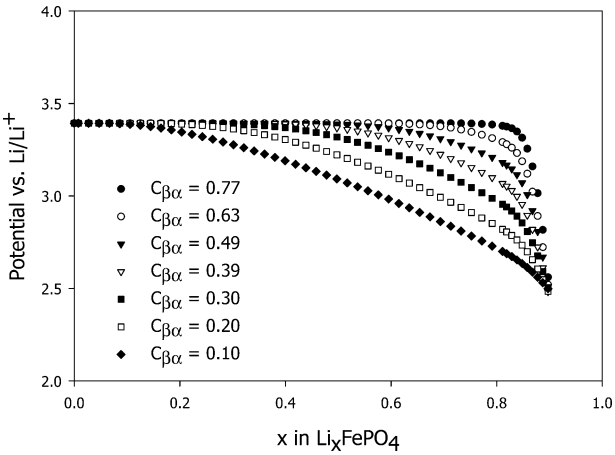

Figure 7. Equilibrium potential curves (obtained from eq 6 with different coefficients) for $LiFePO_4$/A with different solid solution ranges as a function of Li content in $FePO_4$ during discharge process.

for achieving the desired rate capability. For example, in order to achieve 80% or higher rate capability, the diffusion coefficient should be higher than 2×10^{-15} m^2/s and the interface mobility should be higher than 3.1×10^{-11} mmol/(J s). (4) The same rate capability can be achieved at different values of the chemical diffusion coefficient and interface mobility (Figure 6).

Effect of Solid Solution Range and Chemical Diffusion on Rate Capability. Recently, Chiang et al.[6–8] reported that a high rate capability for Nb doped $LiFePO_4$ was attributed to an extended solid solution range. The increase in the solid solution range in $LiFePO_4$ will reduce the crystallographic mismatch[6–8] due to a small concentration difference between $C_{\alpha\beta}$ and $C_{\beta\alpha}$ and will permit coherent phase boundary between the lithiated and delithiated phase. The decrease in the crystallographic mismatch will decrease the accommodation energy, which can be captured in the model by decreasing the A parameter values. To simplify the calculation, the accommodation energy is assumed to decrease linearly with concentration (the value of parameter A was taken as the ratio of $C_{\beta\alpha}$ to 0.77). In the present work, the effect of the solid solution range of $LiFePO_4$ on the

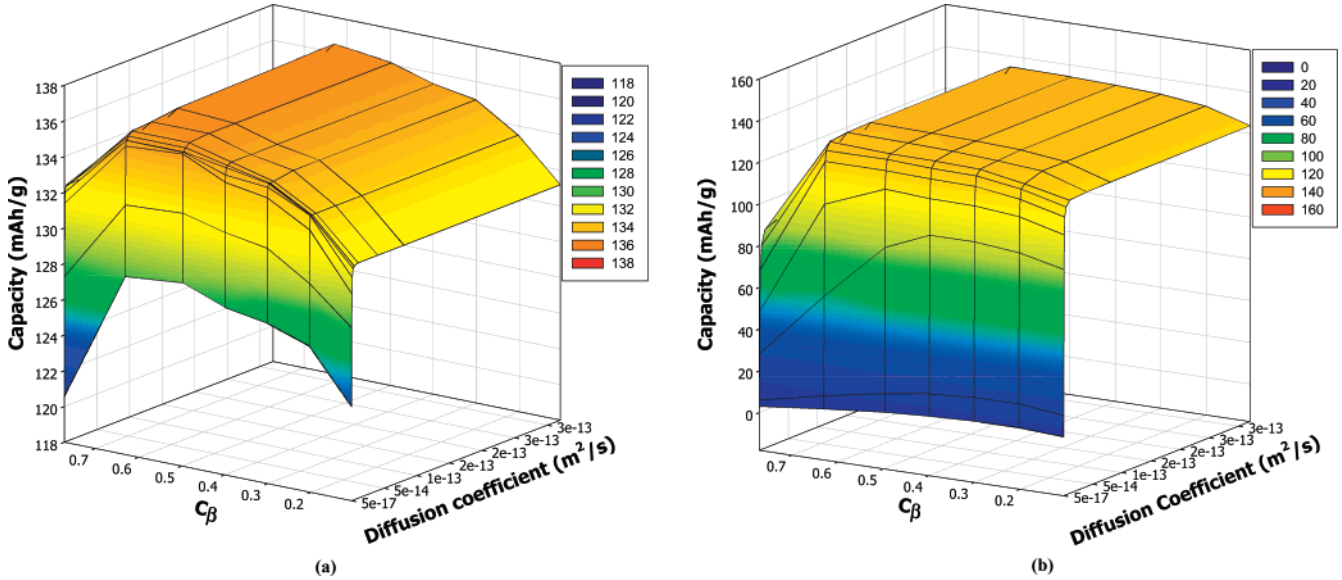

Figure 8. Simulated discharge capacity of $LiFePO_4$/A at different currents as a function of solid solution range and Li chemical diffusion: (a) 0.1 C; (b) 5 C.

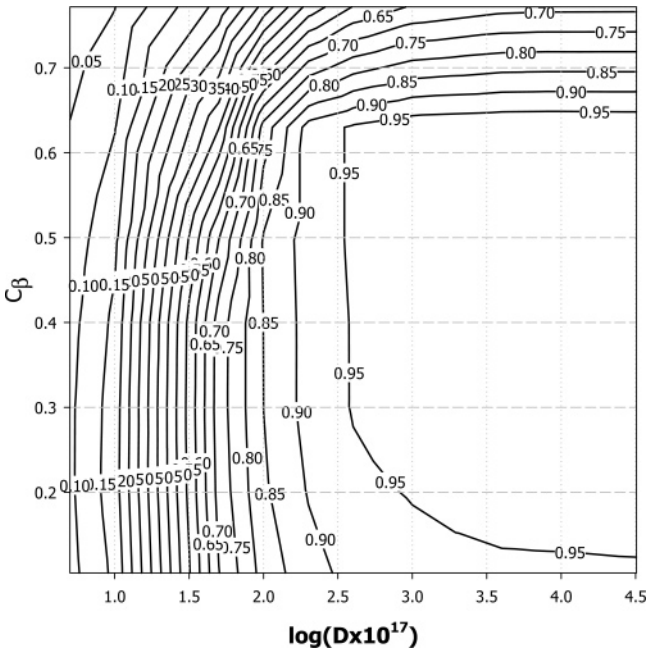

Figure 9. Contour plot for the ratio of discharge capacity (simulated) at 5 C to discharge capacity (simulated) at 0.1 C for $LiFePO_4$/A as a function of chemical diffusion and solid solution range.

rate performance was determined using the proposed model by decreasing the $C_{\beta\alpha}$ from 0.77 to 0.1, i.e., from a phase change material to a large solid solution material. Extending the solid solution range will also decrease the equilibrium concentration of the Li rich phase $C_{\beta\alpha,}$ resulting in an enhanced driving force for interface movement. It will also increase the lithium chemical diffusion rate due to a high concentration difference in the lithiated phase (Figure 1). The change in equilibrium concentration $C_{\beta\alpha}$ can be modeled by changing the coefficients in eq 8. Figure 7 shows the equilibrium potential curves obtained from eq 8, which correspond to $C_{\beta\alpha}$ values of 0.77, 0.63, 0.49, 0.39, 0.30, 0.20, and 0.10. The parameters other than $C_{\beta\alpha}$, D, and A were maintained the same as those of sample A in the simulation. Figure 8 shows 3D graphs for the discharge capacity at 0.1 and 5 C obtained from the model as a function of $C_{\beta\alpha}$ and chemical diffusion coefficient (D). Figure 9 shows the contour plot of rate capability at 5 C as a function of the solid solution range and chemical diffusion for sample A. The discharge behavior of a micron-sized $LiFePO_4$ particle with an interface mobility of 1.3×10^{-11} mmol/(J s) at different solid solution ranges and diffusion coefficient values can be summarized as follows. (1) Irrespective of the chemical diffusion coefficient value, the increase in solid solution range from $C_{\beta\alpha} = 0.77$ to $C_{\beta\alpha} = 0.5$ will improve discharge capacity at 0.1 C (Figure 8a) and rate capability (Figures 8b and 9), which is consistent with the experimental results reported by Chiang et al.[6–8] Interestingly, the discharge capacity at 0.1 C begins to decrease when the electrode material has more than 50% solid solution. Similarly, the rate capability at 5 C was found to decrease when the electrode material has more than 70% solid solution material (Figure 9). This behavior becomes more pronounced at much higher currents (not shown here). The phase transformation during discharge of $LiFePO_4$ has two opposite effects on the discharge rate. On one hand, it induces concentration partitioning at the phase boundary, which results in a faster lithium insertion rate compared to pure lithium chemical diffusion. On the other hand, the accommodation energy induced by the concentration difference between the two phases decreases the phase transformation rate. Therefore, there exists an optimal solid solution range (Figure 9) where the discharge capacity and rate capability reach the maximum. (2) Similarly, the required diffusion coefficient and solid solution values for achieving the desired rate capability can be found from the contour plot. To achieve 80% rate capability at 5 C, micron-size $LiFePO_4$ with an interface mobility of 1.3×10^{-11} mmol/(J s) should have more than 27% solid solution. (3) The same rate capability can be achieved at different solid solution ranges and different chemical diffusion coefficient values. But the highest rate capability and discharge capacity are possible for materials with 50% solid solution range (Figure 9).

Conclusions

A discharge model for phase transformation electrodes controlled by both lithium chemical (ionic and electronic) diffusion and interface mobility was developed. The model was validated by comparing the model discharge curves, at different current densities, with the experimental results of two $LiFePO_4$ samples having different rate capabilities. The rate performance of sample A was mainly controlled by the phase transformation

rate, because its lithium chemical diffusion coefficient estimated from the model was high (8×10^{-14} m^2/s) but the interface mobility (1.3×10^{-11} mmol/(J s)) was too low. sample B has a higher rate capability compared to that of sample A due to increased rate of phase transformation and diffusion coefficient.

To achieve a better rate performance, values of the Li-ion diffusion coefficient (D_{Li}) of $LiFePO_4$ should be higher than 2×10^{-15} m^2/s and the interface mobility should be larger than 1.3×10^{-11} mmol/(J s). For an electrode made of micron-sized particles with moderately low chemical diffusion ability and low solid solution range, it is still possible to achieve a high rate capability by maintaining high interface mobility, i.e., rapid phase transformation rate. Similarly, it is possible to achieve a high rate capability by increasing the solid solution range, though the interface mobility is low. However, the highest rate capability is possible for phase transformation materials with optimum solid solution range, thus making them promising candidates for Li-ion batteries.

Currently, $LiFePO_4$ is available from different manufactures, and surprisingly, all of them exhibit different charge−discharge characteristics and different rate capabilities. This can be explained by the difference in properties such as diffusion, phase transformation, solid solution range, and volume change, which are accounted for in this model. The developed model can be applied to all ion insertion electrodes, therefore making it a useful practical tool in developing the next generation electrode materials.

Acknowledgment. This work was supported by the U.S. army Communications Electronics Command under Contract No. W909MY-06-C-0040. We are thankful to the Center for Manufacturing Research and Department of Chemical Engineering at Tennessee Technological University for their partial financial support during a period of this work. The authors are indebted to Dr. Venkat Subramanian of the Department of Chemical Engineering at Tennessee Technological University for suggestions and discussions on model development and solution approach. Finally, we would like to thank Jianxin Ma for conducting the GITT experiments.

Supporting Information Available: The theory of mixed-mode phase transformation and the calculation of actual interface concentration C_β are included as Supporting Information. The material is available free of charge via the Internet at http://pubs.acs.org.

References and Notes

(1) Padhi, A. K.; Nanjundaswamy, K. S.; Goodenough, J. B. *J. Electrochem. Soc.* **1997**, *144*, 1188.
(2) Huang, H.; Yin, S.-C.; Nazar, L. F. *Electrochem. Solid-State Lett.* **2001**, *4*, A170.
(3) Yang, S.; Song, Y.; Zavalij, P. Y.; Whittingham, M. S. *Electrochem. Commun.* **2002**, *4*, 239.
(4) Chung, S-Y.; Blocking, J. T.; Chiang, Y-M. *Nat. Mater.* **2002**, *1*, 123.
(5) Wang, C.; Hong, J. *Electrochem. Solid-State Lett.* **2007**, *10*, A65.
(6) Chiang, Y-M.; Meethong, N.; Huang, H-Y. S.; Carter, W. C.; Chang, S.; Hsiao, A.; Gozdz, A. S. ECS Meeting, Cancun, Mexico, November 2006.
(7) Meethong, N.; Huang, H.-Y. S.; Speekman, S. A.; Carter, W. C.; Chiang, Y.-M. *Adv. Funct. Mater.* **2007**, *17*, 1115.
(8) Meethong, N.; Huang, H.-Y. S; Speekman, S. A.; Carter, W. C.; Chiang, Y.-M. *Electrochem. Solid-State Lett.* **2007**, *10*, A134.
(9) Doeff, M. M.; x Hu, M. M.; McLarnon, F.; Kostecki, F. *Electrochem. Solid-State Lett.* **2003**, *6*, A207.
(10) Herle, P. S.; Ellis, B.; Coombs, N.; Nazar, L. F. *Nat. Mater.* **2004**, *3*, 147.
(11) Sides, C. R.; Croce, F.; Young, V. Y.; Martin, C. R.; Scrosati, B. *Electrochem. Solid- State Lett.* **2005**, *8*, A484.
(12) Kim, D.-H.; Kim, J. *Electrochem. Solid-State Lett.* **2006**, *9*, A439.
(13) Hong, J.; Wang, C.; Kasavajjula, U. *J. Power Sources* **2006**, *162*, 1289.
(14) Ma, J.; Wang, C.; Wroblewski, S. *J. Power Sources* **2007**, *164*, 849.
(15) Scharner, S.; Weppner, W.; Schmid-Beurmann, P. *J. Electrochem. Soc.* **1999**, *146*, 857.
(16) Ohzuku, T.; Ueda, A.; Yamamoto, N. *J. Electrochem. Soc.* **1995**, *142*, 1431.
(17) Srinivasan, V.; Newman, J. *J. Electrochem. Soc.* **2004**, *151*, A1517.
(18) Chen, G.; Song, X.; Richardson, T. J. *Electrochem. Solid-State Lett.* **2006**, *9*, A295.
(19) Zhang, Q.; White, R. E. *J. Electrochem. Soc.* **2007**, *154*, A587.
(20) Giorgetti, M.; Berrettoni, M.; Scaccia, S.; Passerini, S. *Inorg. Chem.* **2006**, *45*, 2750.
(21) Chen, G.; Song, X.; Richardson T. J. *J. Electrochem. Soc.* **2007**, *154*, A627.
(22) Porter, D. A.; Easterling, K. E. *Phase Transformations in Metals and Alloys*, 2nd ed.; Chapman & Hall: New York, 1992.
(23) Christian, J. *The Theory of Phase Transformations in Metals and Alloys*; Pergamon Press: Oxford, U.K., 1981.
(24) Sietsma, J.; Zwaag, S. V. D. *Acta Mater.* **2004**, *52*, 4143.
(25) Nolfi, F. V.; Shewman, P. G.; Foster, J. S. *Trans. Metall. Soc. AIME* **1969**, *245*, 1427.
(26) Ruiheng, W. U.; Xueyu, R.; Zhang, H.; Hsu, T. Y. *J. Mater. Sci. Technol.* **2004**, *20*, 561.
(27) Sietsma, J.; Mecozzi, M. G.; Bohemen, S. M. C.; Zwaag, S. V. D. *Int. J. Mater. Res.* **2004**, *7*, 356.
(28) Liu, Y. C.; Sommer, F.; Mittemeijer, E. J. *Acta Mater.* **2004**, *52*, 2549.
(29) Nowak, U. *Appl. Numer. Math.* **1996**, *20*, 129.
(30) Zhang, W. *Appl. Numer. Math.* **1996**, *20*, 235.
(31) Bard, A. J.; Faulkner, L. R. *Electrochemical Methods*, 2nd ed.; John Wiley & Sons: New York, 2004; p 99.
(32) Geoffroy, D.; Ravet, N. 21st International Seminar and Exhibit on Primary & Secondary Batteries, Fort Lauderdale, FL, March 2004.
(33) Striebel, K.; Shim, J.; Srinivasan, V.; Newman, J. *J. Electrochem. Soc.* **2005**, *152*, A664.
(34) Whittingham, M. S.; Song, Y.; Lutta, S.; Zavalij, P. Y.; Chernova, N. A. *J. Mater. Chem.* **2005**, *15*, 3362.
(35) Prosini, P. P.; Lisi, M.; Zane, D.; Pasquali, M. *Solid State Ionics* **2002**, *148*, 45.
(36) Yu, D. Y. W.; Fietzek, C.; Weydanz, W.; Donoue, K.; Kurokawa, H.; Fujitani, S. *J. Electrochem. Soc.* **2007**, *154*, A253.
(37) Ellis, B.; Perry, L. K.; Ryan, D. H.; Nazar, L. F. *J. Am. Chem. Soc.* **2006**, *128*, 11416.